[6]Anderson, W. K., Thomas, J. L., and Van Leer, B., "A Comparison of Finite Volume Flux Vector Splittings for the Euler Equations," AIAA Paper 85-0122, Jan. 1985.

[7]Peyret, R., and Taylor, T. D., "Computational Methods for Fluid Flow," Springer-Verlag, New York, 1983, pp. 108-112.

[8]Blottner, F. G., "Accurate Navier-Stokes Results for the Hypersonic Flow over a Spherical Nose Tip," *Journal of Space Crafts*, Vol. 27, No. 2, 1990, pp. 113-122.

Thermal Stratification Effects Near a Vertical Ice Slab in Cold Water

David J. Kukulka*
State University of New York at Buffalo, Buffalo, New York 14222
John Lamb†
Consolidated Edison, Buchanan, New York 10511
and
Joseph C. Mollendorf‡
State University of New York at Buffalo, Buffalo, New York 14260

Introduction

NATURAL convection flows near ice surfaces melting in pure water have been previously studied by various investigators. Codegone[1] was apparently the first to demonstrate convective reversals or inversions around the density extremum. Ede[2] performed the first detailed heat transfer measurements of density inversions.

Wilson and Vyas[3] melted ice in pure water and measured flow velocities using an optical technique that employed a thymol blue pH solution. Their results suggest upward flows for water temperatures below 4.7°C and entirely downward flows for temperatures above 7.0°C. For intermediate temperatures, an oscillatory dual flow regime was indicated. In addition, they found that as the temperature increased from 4.7°C, the oscillatory dual flow phenomenon was increasingly prevalent, with a maximum downward velocity being reached at 5.6°C. Wilson and Lee[4] presented a steady-state, two-dimensional finite difference analysis for the heat and momentum transfer of a semi-infinite vertical ice sheet at 0°C, melting into fresh water. Density varied with local temperature, while the other fluid properties were assumed to be constant and evaluated at the ambient temperature. The results showed three distinctive steady flow regimes characterized by ambient temperatures t_a: upward flow for $t_a \leq 4.5$°C, downward flow for $t_a \geq 6.0$°C, and dual or bidirectional flow for $5.7 \leq t_a \leq 6.0$°C. In the range 4.5°C $< t_a < 5.7$°C, the solution failed to converge. Wilson and Lee[4] suggest that this could be a failure of the steady-state theory being applied to model a phenomena that is inherently unsteady.

El-henawy et al.[5] theoretically studied the laminar boundary-layer flow adjacent to a heated or cooled, vertical flat surface, submerged in unstratified quiescent cold water. Their results demonstrate the existence of multiple steady-state solutions in a natural convection flow. Multiple steady states were discovered in two regions: $0.15149 \leq R \leq 0.15180$ (largely upflow with outside flow reversals) and $0.29181 \leq R \leq 0.45402$ (largely downflow with inside flow reversals). The density extremum parameter R is defined as $(t_m - t_a)/(t_0 - t_a)$, with t_m being the temperature at maximum density and t_0 the ice-liquid interface temperature. It is possible there is a relationship between the multiple steady-state solutions and the observed unsteadiness in this work. For Prandtl number Pr equal to 11.6, El-henawy et al.[5] narrowed the width of the gap where calculations were not possible to $0.1518 < R < 0.29181$. El-henawy et al.[6] developed a new approach to determine the stability of multiple steady-state similarity solutions and applied it to vertical plane surfaces in cold water. Wang and Wang[7] studied a laminar buoyancy-induced plane flow near a vertical ice wall melting in cold pure water. Their computed results show that no solution can be found in the range $0.153298 < R < 0.294322$. Rationale for the existence of this gap is discussed and comparisons are made to previous investigators.[4,5] Hwang et al.[8] presented the first hydrodynamic stability analysis for a vertical plate in cold water in the range $0.29181 \leq R \leq 0.50$. In this range the inside buoyancy force reversals exert a strong influence upon the flow.

Experiments are performed herein to determine the effect of the gradient of thermal stratification on the anomalous unsteadiness near a vertical ice slab melting in cold water. An evaluation of tank-size effects on the influence of the relative configurational stability of the various predicted multiple steady states is made. That is to say, does tank size and/or the associated ambient thermal stratification cause the unsteadiness previously observed. Experiments are performed in the gap, $0.15180 < R < 0.29181$, where numerical calculations were not previously possible, and in the region, $0.29181 \leq R \leq 0.45402$, where multiple steady-state solutions were demonstrated.

Experimental Procedure

The present experimental investigation consisted of the visualization and the determination of the associated melting rates m of the buoyancy-induced flow caused by the melting

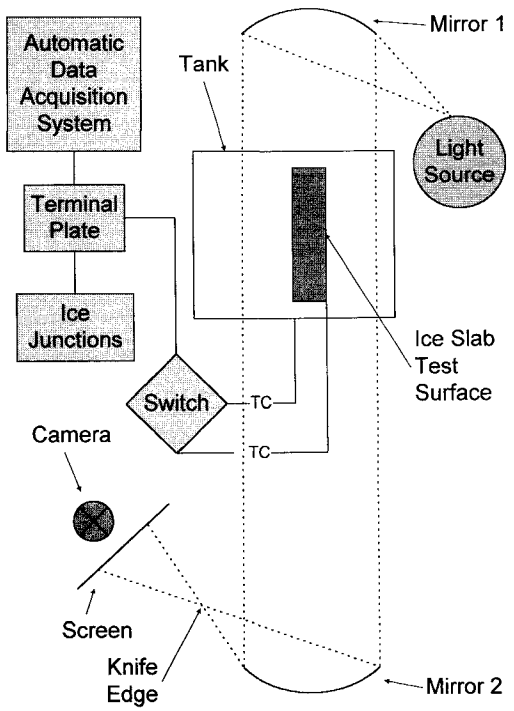

Fig. 1 Experimental layout showing the schlieren optical system.

Received Sept. 20, 1993; revision received Nov. 10, 1994; accepted for publication Nov. 10, 1994.

*Associate Professor, Department of Mechanical Engineering Technology, 1300 Elmwood Ave.

†Project Engineer, Indian Point Station, Broadway & Bleakley Ave.

‡Professor, Department of Mechanical and Aerospace Engineering.

of an ice slab in cold water near its density extremum. The main purpose of these experiments is to observe the anomalous unsteadiness of the flow and determine whether it correlates with thermal stratification. Experiments were performed in two different size tanks.

Ice slab dimensions were 22.9 cm wide by 50.8 cm high with an initial thickness of 3.81 cm. In order to ensure uniform heat flux, the slab was surrounded on the sides by 2.5 cm of expanded styrofoam insulation. To create an ice slab, the framed assembly was filled with de-ionized, degasified water and placed in the middle of a freezer. Both ice surfaces that formed were bubble-free, with straight leading, trailing, and side edges. In order to properly align the slab in the tank, two aligning pins 5 cm long were mounted on the frame.

The larger tank was made of tempered glass measuring 3 m high by 2 m square, insulated with 5 cm of expanded polyurethane foam and covered with plywood. The smaller tank was made of stainless steel measuring 0.86 m high by 0.61 m square and was also insulated and covered. Ambient water temperature could be adjusted using a constant flow chiller and vigorously stirring the water. When the desired ambient temperature was reached, the tank was allowed to stand for 60 min in order to let viscous effects damp out the residual motion from the stirring. Six Copper/Constantan thermocouples were used to check the degree of thermal stratification in the tank throughout the experiment. All thermocouple signals were sent to a data acquisition system (see Fig. 1 for the general arrangement). The ice slab was suspended by a hook from a Mettler Model PE 4000 balance. In order to counteract buoyancy, a weight of 2.2 kg was suspended from the frame surrounding the submerged slab. When the ice slab was aligned properly with the optical system, the aligning pins appeared to have equal lengths on the viewing screen. After immersion, the ice was allowed to melt for 5 min in order to allow the transient affects to die out. A vertical knife edge was used to optimally observe the density gradient in the horizontal direction. Using a motor-driven Nikon MD-2 camera, controlled by a programmable Nikon MT-1 intervalometer, sequential photographs were taken of the flow visualized by the schlieren optical system.

Experimental Results

An experimental run consisted of an ice slab, initially at 0°C throughout, being immersed in water at an ambient temperature t_a. The instantaneous weight readings M were recorded throughout the experiment. Weight change results vs time, at specified R values, were also recorded. Slopes of this data were converted to a melting rate m by considering the buoyancy effect of the ice and using the density of pure water, at t_a and 1 atm, from the density relation of Gebhart and Mollendorf.[9]

By knowing the melting rate m at the ambient temperature, the Nusselt number $\bar{N}u$, can be calculated using $\bar{N}u = (mh_{il})/[2wk(t_a - t_0)]$ as presented by Hwang.[10] Here, w is the width of the ice slab, k the thermal conductivity evaluated at the film temperature, and h_{il} the latent heat of fusion.

The thermal stratification was determined using the temperature history and the distance between thermocouples.

Overall mean stratification X was calculated for each run using

$$X = \frac{1}{j}\sum_{i=1}^{i=j} \bar{S}_i \tag{1}$$

where

$$\bar{S} = \frac{1}{n}\sum_{i=1}^{i=n} \frac{T_i - T_{i+1}}{d_{i+1} - d_i}$$

and T is a thermocouple reading, d the location of the thermocouple from the top of the tank, n the number of thermocouples $- 1$, and j the (total time of the run/30) $+ 1$.

Standard deviation S' could be determined from

$$S' = \left\{\sum_{i=1}^{i=j} \frac{S_i - X^2}{j}\right\}^{1/2} \tag{2}$$

Nondimensional heat transfer rate, $\varphi'(0)$, is related to the experimental Nu and Grashof number Gr_L using

$$-\varphi'(0) = (3\sqrt{2}\bar{N}u)/4(Gr_L)^{1/4} \tag{3}$$

Results (taken from Table 1) of the $-\varphi'(0)$ are plotted against R in Fig. 2 and compared to relations given in Elhenawy et al.[5] The data clearly tends to favor the upper branch of the largely downflow region regardless of the degree of thermal stratification. This seems to suggest that the flows observed here are not fluctuating between two steady states. The dotted line connecting points L2 and L3 in Fig. 2 suggest a steady-state path in the gap, $0.15180 < R < 0.29181$, where numerical calculations are not possible. Although the path is highly speculative, it is perhaps the best possible information available at this time.

Sequential photographs taken of the flow visualized by the schlieren optical system are presented in Fig. 3 for representative conditions in the large and small tanks. These photographs document the flow visualized, with the ice surface being indicated on the photographs as well as the direction of gravity. The boundary layer appears adjacent to the ice surface (to the reader's right) and is white. These photographs represent an integrated view, as visualized by the schlieren optical system. In Figs. 3a–3c an anomalous unsteadiness can be seen; whereas the sequence of photographs in Figs. 3d–3f does not show an anomalous unsteadiness.

In Figs. 3a–3c (small tank), the flow direction cannot be determined, however, the unsteadiness of the flow can be

Table 1 Heat transfer results for various experimental conditions

Run/tank size	t_a, °C/R	$\bar{N}u$	m, g/s	h, W/m² °C/Gr_L	$-\varphi'(0)$	$\bar{S}$, °C/m/S'
S1	6.09	84.24	0.4025	94.85	0.824	1.49
Small	0.3378			1.3797×10^8		0.072
S2	4.80	77.84	0.2921	87.34	0.861	1.50
Small	0.1615			8.4735×10^7		0.082
S3	5.84	69.80	0.3198	78.59	0.697	1.71
Small	0.3100			1.2744×10^8		0.055
L1	6.05	80.97	0.3860	91.17	0.795	0.05
Large	0.3340			1.3629×10^8		0.011
L2	5.00	77.93	0.3065	87.59	0.842	0.06
Large	0.1940			9.2684×10^7		0.038
L3	5.60	71.39	0.3150	80.39	0.729	0.03
Large	0.2805			1.1629×10^8		0.018

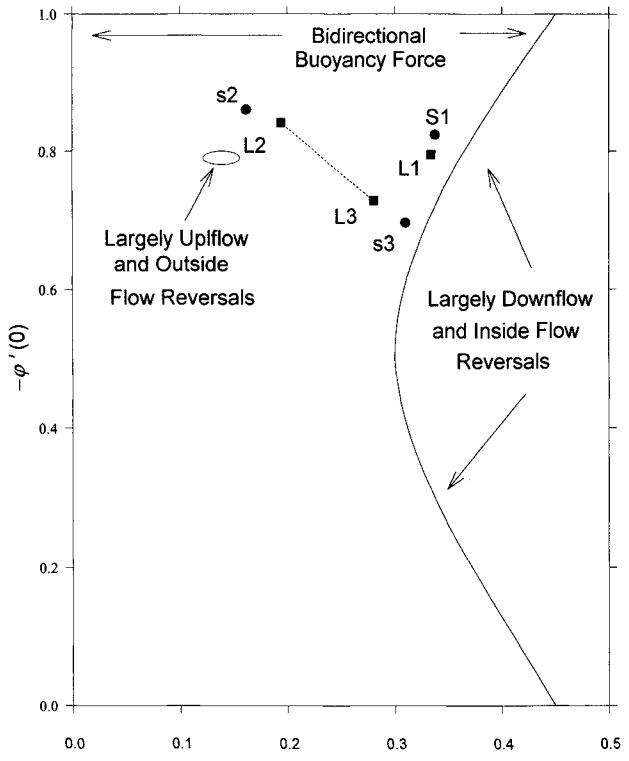

Fig. 2 Comparison of nondimensional heat transfer data to the results presented by El-henawy et al.[5]

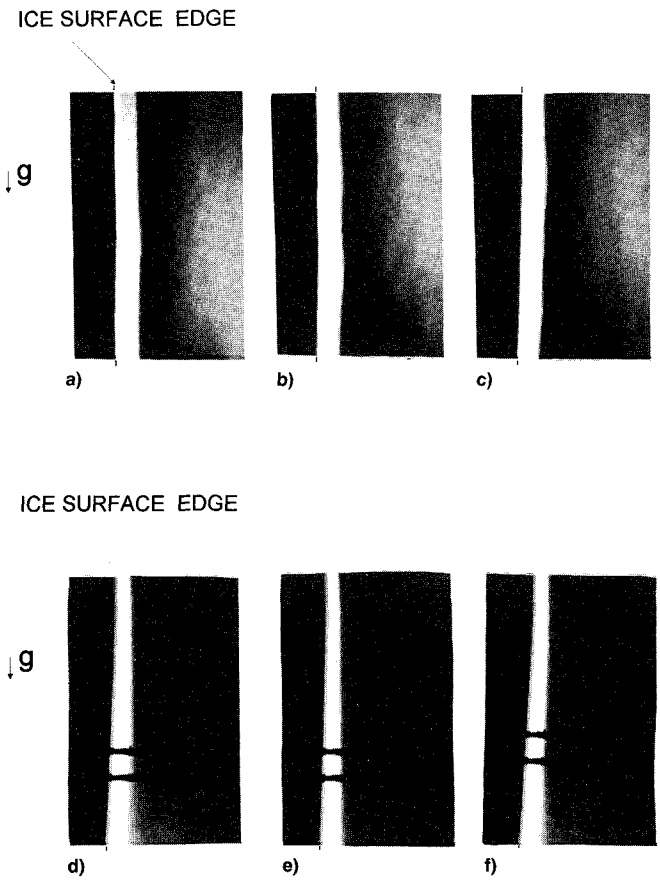

Fig. 3 Representative sequence of photographs taken in the small tank showing anomalous unsteadiness for R = 0.3378 and a stratification = 1.49°C/m. For time = a) 90, b) 210, and c) 780 s. d)–f) Large tank showing no anomalous unsteadiness for R = 0.3340 and a stratification = 0.05°C/m. For time = d) 60, e) 210, and f) 790 s.

determined by the presence of "waves" on the outer edge of the boundary layer. Waves are seen at 90 s and have moved upward at 210 s, with waves also being seen at 780 s. Therefore, for R = 0.3378 with a stratification = 1.49°C/m, the flow was unsteady. Similar unsteady flow patterns were also visualized in runs s2 (R = 0.1615 with a stratification = 1.50°C/m) and s3 (R = 0.3100 with a stratification = 1.71°C/m). The unsteadiness of the flow visualized during run s3 was not as dramatic as the unsteadiness seen in run s1. This is probably due to the relative closeness of the data point to the upper branch of the theoretically determined steady-state curve in Fig. 2.

The flow direction in Figs. 3d–3f cannot be determined; however, the steadiness of the flow is shown by the absence of waves on the outer edge of the boundary layer. Here, the boundary layer has no visible waves and appears to be relatively steady throughout the photographic sequence. Therefore, at R = 0.3340, with a stratification = 0.05°C/m, the flow was determined to be steady. Steady flow patterns were also observed for runs L2 (R = 0.1940 with a stratification = 0.06°C/m) and L3 (R = 0.2805 with a stratification = 0.03°C/m).

The results of this study suggest a relationship between the thermal stratification within the tank and the observed anomalous unsteadiness. When the stratification was high (1.49, 1.51, and 1.71°C/m), an anomalous unsteadiness arose, as shown in Figs. 3a–3c. When the stratification was low (0.05, 0.06, and 0.03°C/m), an anomalous unsteadiness did not arise, as shown in Figs. 3d–3f.

Conclusions

In the present study, the flows in the small tank were unsteady, while the flows in the large tank were steady. Representative photographs in Fig. 3 clearly show these flow conditions with Table 1 summarizing the experimental results. The thermal stratification in the small tank was approximately 50 times greater than the thermal stratification of similar runs in the large tank. This suggests the degree of thermal stratification has a strong effect, but may not necessarily be the only factor influencing the anomalous unsteadiness. Another possible factor that could be influencing the unsteadiness is the tank size itself, independent of the thermal stratification.

References

[1]Codegone, C., "Su un punto d'inversione dei moti convetivi," *Accademia Delle Scienze Di Torino*, Vol. 75, 1939, p. 167.

[2]Ede, A. J., "Heat Transfer by Natural Convection in Refrigerated Liquid," *Proceedings of the 8th International Conference on Progress in Refrigeration*, International Inst. of Refrigeration, London, 1951, p. 260.

[3]Wilson, N. W., and Vyas, B. D., "Velocity Profiles Near a Vertical Ice Surface Melting into Fresh Water," *Journal of Heat Transfer*, Vol. 101, No. 2, 1979, pp. 313–317.

[4]Wilson, N. W., and Lee, J. J., "Melting of a Vertical Ice Wall by Free Convection into Fresh Water," *Journal of Heat Transfer*, Vol. 103, No. 1, 1981, pp. 13–17.

[5]El-henawy, I., Hassard, B., Kazarinoff, N., Gebhart, B., and Mollendorf, J., "Numerically Computed Multiple Steady States of Vertical Buoyancy-Induced Flows in Cold Pure Water," *Journal of Fluid Mechanics*, Vol. 122, Sept. 1982, pp. 235–250.

[6]El-henawy, I., Hassard, B., and Kazarinoff, N., "A Stability Analysis of Non-Time-Period Perturbations of Buoyancy-Induced Flows in Pure Water Near 4°C," *Journal of Fluid Mechanics*, Vol. 163, Feb. 1986, pp. 1–20.

[7]Wang, C. A., and Wang, S. J., "Multiple Similarity Solutions of Buoyancy Induced Flows for Ice Melting in Cold Pure Water," *Computers and Mathematics with Applications*, Vol. 15, No. 12, 1988, pp. 1007–1017.

[8]Hwang, Y., Kazarinoff, N., and Mollendorf, J. C., "Hydrodynamic Stability of Multiple Steady-States of Vertical Buoyancy-Induced Flows in Cold Pure Water," *International Journal of Heat and Mass Transfer*, Vol. 36, No. 2, 1993, pp. 423–435.

[9]Gebhart, B., and Mollendorf, J. C., "A New Density Relation for Pure and Saline Water," *Deep-Sea Research*, Vol. 24, No. 9, 1977, pp. 831–848.

[10]Hwang, Y., "The Stability of Some Steady-States and the Effect of Motion Pressure in Vertical Natural Convection Flows in Cold Water," Ph.D. Dissertation, State University of New York, Buffalo, NY, 1984.

Implicit Solution Method for a Cumulative Variable Formulation to Radiative/Conductive Transport

J. I. Frankel*
University of Tennessee,
Knoxville, Tennessee 37996-2210

I. Introduction

In a recent article,[1] a new formulation was presented for transient, one-dimensional conductive and radiative transport in a gray, plane-parallel medium. The introduction of cumulative variables[2,3] and the subsequent use of a concept offered by Kumar and Sloan[4] permitted the complicated integro-differential formulation to be readily and accurately resolved by orthogonal collocation. Several questions naturally arise with regard to computation, and thus, these issues deserve attention early in the developmental stages. Germane to this Note is the unfolding of an efficient numerical method for resolving the unknown expansion coefficients[1] presented by the collocation approach.

This Note presents an implicit numerical method for solving the time-varying expansion coefficients developed by Frankel.[1] Thus, the focus is directed toward the presentation of an efficient and accurate block-by-block method[5–7] for solving a system of nonlinear Volterra integral equations of the second kind. Finally, some new numerical results are presented when the single-scattering albedo is zero and unity.

II. Implicit Formulation and Analysis

For the sake of uniformity, the nomenclature used in this Note is identical to that presented in Ref. 1. Additionally, since this Note addresses only the computational methodology associated with resolving the expansion coefficients expressed by Frankel,[1] only details concerning these functions are presented. Reconstruction of the needed solutions is shown by Frankel.

The coupled, differential/algebraic matrix system of equations for the expansion coefficients of the three cumulative variables $\{\Psi_k^N(\eta, \xi)\}_{k=1}^3$ described by Frankel are

$$B\frac{d\bar{a}}{d\xi}(\xi) = \bar{g}(\xi) \tag{1a}$$

$$B\frac{d\bar{b}}{d\xi}(\xi) = \bar{h}(\xi), \qquad \xi > 0 \tag{1b}$$

$$A\bar{c}(\xi) = \bar{f}(\xi), \qquad \xi \geq 0 \tag{1c}$$

where $\bar{a}(\xi) = [a_0^N(\xi), a_1^N(\xi), \ldots, a_N^N(\xi)]^T$, $\bar{b}(\xi) = [b_0^N(\xi), b_1^N(\xi), \ldots, b_N^N(\xi)]^T$, and $\bar{c}(\xi) = [c_0^N(\xi), c_1^N(\xi), \ldots, c_N^N(\xi)]^T$. The elements of the $(N+1) \times (N+1)$ coefficient matrix B, as presented in Ref. 1, are

$$b_{jm} = T_m(\eta_j), \quad j = 0, 1, \ldots, N \quad m = 0, 1, \ldots, N \tag{1d}$$

The vectors $\bar{g}(\xi) = [g_0^N(\xi), g_1^N(\xi), \ldots, g_N^N(\xi)]^T$ and $\bar{h}(\xi) = [h_0^N(\xi), h_1^N(\xi), \ldots, h_N^N(\xi)]^T$ have components

$$g_0^N(\xi) = \theta_2 \tag{1e}$$

$$g_j^N(\xi) = \theta_i + \frac{1}{\alpha^2}\sum_{m=0}^{N} a_m^N(\xi)T_m''(\eta_j) - \frac{(1-\omega)}{N_{cr}}\sum_{m=0}^{N}[b_m^N(\xi) - c_m^N(\xi)]T_m(\eta_j)$$

$$j = 1, 2, \ldots, N-1 \tag{1f}$$

$$g_N^N(\xi) = 1 \tag{1g}$$

while

$$h_j^N(\xi) = [g_j^N(\xi)]^4, \qquad j = 0, 1, \ldots, N \tag{1h}$$

The components of the $(N+1) \times (N+1)$ coefficient matrix A are

$$a_{jm} = T_m(\eta_j) - (\alpha\omega/2)A_m^{\alpha}(\eta_j)$$

$$j = 0, 1, \ldots, N, \quad m = 0, 1, \ldots, N \tag{1i}$$

The unknown time-varying components in $\bar{f}(\xi) = [f_0^N(\xi), f_1^N(\xi), \ldots, f_N^N(\xi)]^T$ are given as

$$f_j^N(\xi) = h(\eta_j, \xi) + \frac{\alpha(1-\omega)}{2}\sum_{m=0}^{N} b_m^N(\xi)A_m^{\alpha}(\eta_j)$$

$$j = 0, 1, \ldots, N \tag{1j}$$

Here, $T_m(\eta)$ represents the mth Chebyshev polynomial for the first kind, and η_j represents the jth collocation point as given in Ref. 1. The function $h(\eta_j, \xi)$ and constants $A_m^{\alpha}(\eta_j)$ are presented by Frankel.[1]

Though notationally not explicit, it is clear from viewing the definitions of the vector functions $\bar{f}(\xi)$, $\bar{g}(\xi)$, and $\bar{h}(\xi)$ that coupling exists among the unknown time-varying expansion coefficients of the cumulative variables. The physical variables can be reconstructed[1] once satisfactory numerical closure on the cumulative variables has been ordained.

The unknown expansion coefficients for $\Psi_3^N(\eta, \xi)$ are denoted by $\{c_m^N(\xi)\}_{m=0}^N$. These functions can be symbolically resolved in terms of the functions $\{a_m^N(\xi)\}_{m=0}^N$ and $\{b_m^N(\xi)\}_{m=0}^N$ using *Mathematica*™.[8] Formally, this is done through an inverse operation, i.e.,

$$\bar{c}(\xi) = A^{-1}\bar{f}(\xi), \qquad \xi \geq 0 \tag{2}$$

when $|A| \neq 0$. Thus, the components of the vector $\bar{c}(\xi)$ can be eliminated from $\bar{g}(\xi)$ and $\bar{h}(\xi)$. This, in effect, reduces the differential/algebraic matrix system shown in Eqs. (1a–1c) to a pure differential matrix system. Equations (1a) and (1b) constitute the starting point for the development of the implicit numerical method. This approach is taken due to the already noted stability constraints imposed on the initial value scheme as the order of the approximation is increased.[1] In Ref. 1, a fully explicit fifth-order Runge–Kutta method was used in solving the time-varying expansion coefficients $\{a_m^N(\xi)\}_{m=0}^N$ and $\{b_m^N(\xi)\}_{m=0}^N$. As noted,[1] the time steps required in an explicit method must decrease in size as N increases in order to ensure convergence. To overcome this

Received Oct. 28, 1994; revision received Dec. 17, 1994; accepted for publication Jan. 24, 1995.

*Associate Professor, Mechanical and Aerospace Engineering Department.